ELSEVIER

Remote Sensing of Environment 76 (2000) 181–201

Remote Sensing of Environment

www.elsevier.com/locate/rse

Fine structure of the celestial polarization pattern and its temporal change during the total solar eclipse of 11 August 1999

István Pomozi[a], József Gál[a], Gábor Horváth[a,*], Rüdiger Wehner[b]

[a]*Department of Biological Physics, Eötvös University, Pázmány sétány 1, Budapest H-1117, Hungary*
[b]*Zoologisches Institut, Universität Zürich, Winterthurerstrasse 190, Zurich CH-8057, Switzerland*

Received 29 June 2000; accepted 6 November 2000

Abstract

Using 180° field-of-view (full-sky) imaging polarimetry, we measured the spatiotemporal change of the polarization pattern of the entire celestial hemisphere during the total solar eclipse of 11 August 1999 in Kecel, Hungary. We compared these patterns with the normal celestial polarization patterns measured at the same times on the subsequent day of the eclipse. As a second control sky, the celestial polarization pattern measured on 26 August 1999 in Tunisia was chosen with the same solar zenith distance as that at the Hungarian eclipse. We computed the corresponding theoretical celestial polarization patterns on the basis of the single-scattering Rayleigh model. The spectral characteristics of the polarization pattern in the sky during totality were also measured in the red (650 nm), green (550 nm), and blue (450 nm) ranges of the spectrum. A qualitative explanation was given for the origin of the angle of polarization (***E***-vector) pattern and the neutral point of skylight polarization near the zenith observed during totality. The relation of our results to earlier observations on skylight polarization during total eclipses was analyzed. The agreements with previous eclipse observations were discussed. The reasons for some disagreements with previous eclipse observations were explained in connection with the spectral dependence of skylight polarization and the fine structure of the celestial ***E***-vector pattern during totality.

Keywords: Atmospheric optics; Celestial polarization pattern; Total solar eclipse; 180° field-of-view imaging polarimetry; Change of skylight polarization

1. Introduction

A total solar eclipse is one of the most spectacular natural phenomena. During such an eclipse, the sun is completely covered by the moon for some minutes, and this immediately transforms the aspect of the sky completely. Then the sky is not lit up by the radiance of the solar corona alone; the main source of skylight is light coming from outside the area where the totality is taking place and where the sun is still shining. This is never farther away from the observer than about 130 km (Können, 1985). During a total eclipse, a particular type of twilight occurs: Most of the light is seen near the horizon where parts of the atmosphere are still lit by the partially eclipsed sun outside the zone of totality, and the sky is darkest in the zenith.

Since the beginning of the 1960s, several atmospheric optical phenomena associated with total solar eclipses have been the subject of extensive studies (e.g., Coulson, 1988): The rapid change in light intensity of the sky, the apparent sudden darkening at totality, the peculiar quality of the atmospheric light, and the change in sky colour during totality have frequently been noted, described, commented on, and measured. Increasingly accurate measurements of skylight intensity and colour have also been made. It was not, however, until the total solar eclipse of 15 February 1961 that the change in sky polarization during totality was observed by de Bary, Bullrich, and Lorenz (1961). Subsequently, this phenomenon has been sporadically studied.

As the brightness and colour distribution of light of the sky are immediately transformed at totality, so also is the polarization of skylight. Apart from the very scant light of the solar corona, the direct sunlight is cut off during a total eclipse; thus, the skylight is produced almost entirely by secondary and higher-order scattering (Fig. 8A), in which case, the degree of polarization of skylight should be very low. The knowledge accumulated about the celestial polarization during total solar eclipses is rather modest. The

* Corresponding author. Tel.: +36-1-372-2765; fax: +36-1-372-2757.
E-mail address: gh@arago.elte.hu (G. Horváth).

0034-4257/00/$ – see front matter
PII: S0034-4257(00)00203-0

Table 1
Parameters of the Hungarian total solar eclipse of 11 August 1999 and the places of the polarimetric measurements

Date of total solar eclipse	11 August 1999
Percentage of totality	102.9%
Solar zenith distance	32°
Velocity of the umbra along the path of totality	680 m/s = 2450 km/h
Major axis of the elliptical umbra	113 km
Minor axis of the elliptical umbra	96 km
Time of first contact (beginning of the partial eclipse)	11:28:35 (local summer time = UTC + 2)
Second contact (beginning of the total eclipse)	12:51:34
Midtotality	12:52:45
Third contact (end of the total eclipse)	12:53:56
Fourth contact (end of the partial eclipse)	14:15:35
Observation site	Kecel (Hungary)
Latitude	46°32′ North
Longitude	19°16′ East
Date of control measurements in Kecel (Control 1)	12 August 1999
Date and time of control measurements in Tunisia (Control 2)	26 August 1999, 12:00:00 (local summer time = UTC + 1)
Solar zenith distance	32°
Observation site	Chott el Djerid, 10 km from Kriz (Tunisia)
Latitude	33°52′ North
Longitude	8°22′ East

reason for this is that, until now, it was not possible to measure the polarization pattern of the entire sky during the few minutes of a total eclipse. The few skylight polarization measurements performed until now, during total eclipses, used point-source photopolarimeters with fields of view not wider than a few degrees, oriented usually in the direction of the zenith and/or at 90° from the sun in the sun's vertical.

de Bary et al. (1961) measured the temporal change of the degree of polarization of skylight at 90° from the obscured sun during the total solar eclipse of 15 February 1961 in Viareggio, Italy. Dandekar and Turtle (1971) performed skylight polarization measurements in the blue and red spectral ranges at a point 90° from the sun during the total eclipse of 7 March 1970 in Kinston, USA. Shaw (1975) measured the polarization of skylight in the blue range of the spectrum in the sun's vertical and perpendicularly to the solar meridian during the 30 June 1973 total eclipse in Kenya, Africa. Using two polarimeters oriented in the direction of the zenith and at 90° from the sun in the sun's vertical, Coulson (1988) observed a virtual lack of polarization response during a partial (approximately 80%) eclipse of the sun at Davies, USA on 26 February 1979.

To our knowledge, little more than cited information about celestial polarization during total eclipses is not available due to a lack of wide-field skylight measurements. Using a single-channel ($\lambda = 400$ nm) rotating analyzer, point-source polarimeter with a field of view of $1.44 \times 5.44°$ during totality, Shaw (1975) was able to make repeated scans in the solar vertical plane and in a vertical plane crossing the zenith perpendicular to the solar meridian. However, this scanning could not compensate for the lack of a wide field-of-view polarimeter. Apart from the work of Shaw, there is no report on measurements of the distribution of brightness, colour, and polarization with angle on the celestial hemisphere, i.e., on the variation of the Stokes parameters in different viewing directions during totality. Recently, North and Duggin (1997) designed a rather voluminous and cumbersome photopolarimeter for obtaining partial Stokes vectors and derivative images of the skydome by taking advantage of a four-lens photographic camera and a spherical convex mirror. Another easier method was developed by Voss and Liu (1997) for measuring full-sky polarization patterns. More recently, using a photographic camera with a 180° field-of-view fisheye lens equipped with three differently oriented linearly polarizing filters, Gál, Horváth, and Meyer-Rochow (2001) developed a similar technique, by which the polarization pattern of the entire celestial hemisphere can be easily and rapidly measured.

Using the latter technique, an opportunity to measure the temporal change of the polarization pattern of the entire celestial hemisphere during the total solar eclipse of 11 August 1999 occurred in Hungary. We measured the celestial polarization pattern from the beginning of the partial eclipse through the totality to the end of the partial eclipse. We compared these patterns with the normal celestial polarization patterns measured at the same times on the subsequent day of the total eclipse. As a second control sky, the celestial polarization pattern measured on 26 August 1999 in Tunisia was chosen with the same solar zenith distance as that at the Hungarian eclipse. We computed also the corresponding theoretical celestial polarization patterns on the basis of the single-scattering Rayleigh model.

As far as we know, the temporal change of the polarization pattern of the entire sky during a total solar eclipse has never been measured previously. Although the main characteristics of the normal polarization of the firmament are well known (Coulson, 1988; Gál et al., 2001; Horváth, Gál, Pomozi, & Wehner, 1998; Horváth & Wehner, 1999; Können, 1985; North & Duggin, 1997), the same cannot be said

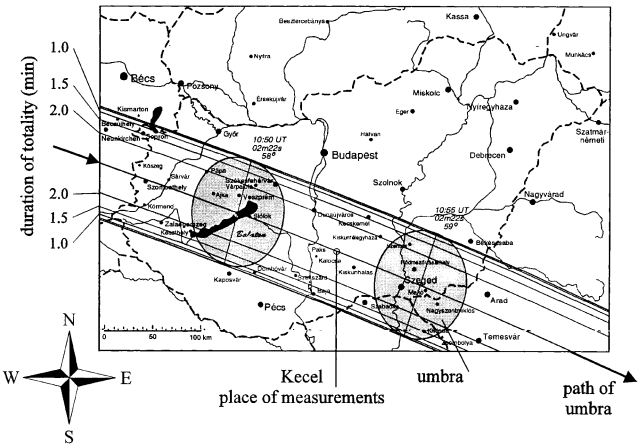

Fig. 1. Map of Hungary showing the path of the moon's shadow and its elliptical intersection (umbra) with the ground during the total solar eclipse of 11 August 1999.

about the fine structure of the celestial polarization pattern and its temporal change during total solar eclipses. The aim of this work is to partially fill this gap. Since the change and characteristics of skylight intensity and colour during total eclipses are thoroughly studied and well documented in the literature, in this work, we restrict ourselves to measurements of the degree of polarization and ***E***-vector alignment (angle of polarization) of skylight.

2. Materials and methods

2.1. Places and dates of the measurements

The parameters of the Hungarian total solar eclipse of 11 August 1999 and the places and dates of the polarimetric measurements are summarized in Table 1. Our measurements were performed in Southern Hungary, in the immediate vicinity of the village Kecel on 11 August 1999 when a total solar eclipse occurred (Fig. 1). This place was practically on the centre line of the path of the moon's shadow (umbra) sweeping the Earth's surface. At the place of our measurements, the beginning of the partial eclipse, the beginning of the total eclipse, the end of the total eclipse, and the end of the partial eclipse were 11:28:35, 12:51:34, 12:53:56, and 14:15:35 (local summer time = UTC + 2), respectively. Fortunately, the atmosphere was clear from the beginning to the end of the partial eclipse after a cold-front passage prior to the beginning of the partial eclipse.

On 12 August 1999, we measured the celestial polarization pattern at the same place (Kecel) and times as on 11 August. This series served as Control 1. Unfortunately, at Kecel, after 11 August, the sky was always more or less partially cloudy between 11:28:35 and 14:15:35; thus, we could not record a control series of clear skies at Kecel. Therefore, we developed a simple computer algorithm to recognize the clouds on the pictures of the sky. Using this algorithm, the cloudy areas of the sky could be filtered out; thus, only the clear sky regions were taken into consideration in the comparison with the eclipse series recorded on 11 August 1999.

As Control 2, we used the celestial polarization pattern measured at 12:00:00 on 26 August 1999 in the Tunisian Chott el Djerid, 10 km from the village Kriz (see Table 1). At this time and arid site, the sky was clear and the solar zenith distance of 32° was the same as that during the Hungarian total eclipse. In the comparison between this Tunisian celestial polarization pattern and the Hungarian eclipse skies, the former was always appropriately rotated in such a way that the sun coincided with the partially or totally eclipsed sun of the Hungarian skies.

Table 2
Times of exposure, apertures, and types of photographic film, with which the sky was photographed during the different polarimetric measurements

	Pre-eclipse	Pre-eclipse	Pre-eclipse	Pre-eclipse	Eclipse	Eclipse	Eclipse	Posteclipse	Posteclipse	Posteclipse
Recording time	12:45:00	12:48:00	12:50:00	12:51:00	12:51:34	12:52:00	12:52:30	12:59:00	13:01:00	13:02:00
Percent obscuration of sun's disk (%)	90.4	95.0	98.0	99.4	100	100	100	92.2	89.0	87.5
Eclipse (Kecel, Hungary)										
Exposure time (s)	1/30	1/15	1/8	1/8	1/4	1/2	1	1/30	1/60	1/60
Aperture (*f*-number)	8	8	2.8	2.8	2.8	2.8	2.8	8	8	8
Photographic film	F400	F400	F400	F400	K1600	K1600	K1600	F400	F400	F400
Control 1 (Kecel, Hungary)										
Exposure time (s)	1/500	1/500	1/500	1/500	1/500	1/500	1/500	1/500	1/500	1/500
Aperture	8	8	8	8	8	8	8	8	8	8
Photographic film	K200	K200	K200	K200	K200	K200	K200	K200	K200	K200
Control 2 (Chott el Djerid, Tunisia)										
Exposure time (s)	1/500	1/500	1/500	1/500	1/500	1/500	1/500	1/500	1/500	1/500
Aperture	5.6	5.6	5.6	5.6	5.6	5.6	5.6	5.6	5.6	5.6
Photographic film	F100	F100	F100	F100	F100	F100	F100	F100	F100	F100

Colour reversal films used were the following: F100: Fujichrome Sensia II 100 ASA, F400: Fujichrome Sensia II 400 ASA, K200: Kodak E 200 ASA, K1600: Kodak EPH 1600 ASA.

2.2. Measurement of the entire celestial polarization pattern by 180° field-of-view rotating analyzer imaging photopolarimetry

The polarization pattern of the entire celestial hemisphere was measured by 180° field-of-view (full-sky) rotating analyzer imaging photopolarimetry, the details of which are described by Gál et al. (2001). The recording was taken by a Nikon F801 photographic camera equipped with a Nikon-Nikkor (*f*: 2.8, focal length: 8 mm, field of view: 180°) fisheye lens including a built-in rotating disc mounted with three neutral density linearly polarizing (HNP′B) filters with three different polarization axes (0°, 45°, and 90° measured from the radius of the disc). Table 2 summarizes the times of exposure, apertures, and types of photographic film, with which the sky was photographed. From a given sky, three photographs were taken for the three different alignments (0°, 45°, 90°) of the transmission axis of the polarizers on the built-in rotating disc. As detectors, we used Fujichrome Sensia II (100, 400 ASA) and Kodak E, EPH (200, 1600 ASA) colour reversal films. Table 3 summarizes the spectral sensitivity characteristics of these films. The camera was set up on a tripod in such a way that its axis passing through the viewfinder pointed northward, and the optical axis of the fisheye lens was vertical. In order to eliminate the distorting internal reflections of direct sunlight from the refracting surfaces of the fisheye lens during the partial eclipse and the control measurements, the sun was screened out by a small disk, which could be slid along a circular wire positioned radially and concentrically with respect to the outer (entrance) surface of the lens (see, e.g., Fig. 2A1).

With the aid of a personal computer, after digitization (with a Hewlett-Packard ScanJet 6100C) and evaluation of the three developed slides belonging to a given sky, the patterns of the brightness, degree of polarization, and ***E***-vector alignment of skylight were determined and visualized as high-resolution, colour-coded, two-dimensional circular patterns in the red, green, and blue spectral ranges, in which the three colour-sensitive layers of the used photoemulsions have the maximal sensitivity (Table 3). The subsequent computer evaluation of the three digitized colour photographs of the firmament obtained by our full-sky imaging photopolarimeter was practically the same as in the case of videopolarimetry described earlier by Horváth et al. (1998), Horváth and Varjú (1997), and Horváth and Wehner (1999).

Table 3
Maxima (at wavelengths λ_x, x = red, green, blue) and half-band widths of the spectral sensitivity curves of the photographic films used in the polarimetric measurements

	F100, F400, K200, K1600
λ_{red} (nm)	650 ± 30
λ_{green} (nm)	550 ± 30
λ_{blue} (nm)	450 ± 50

The designations of the colour reversal films are the same as in Table 2.

Our imaging polarimeter was calibrated. The reliability of the process of development of the colour reversal films was ensured in such a way that the films were developed always in the same professional Kodak laboratory in Budapest using the same automatically controlled method. In the evaluation of the recordings, i.e., in the calculation of the brightness, degree, and angle of polarization of skylight, the following characteristics of the recording and digitizing system were taken into consideration: (i) the measured Mueller matrix of the fisheye lens as a function of the angle of incidence with respect to the optical axis; (ii) the measured angular distortion of the fisheye lens vs. the angle of incidence; (iii) the decrease of light intensity imaged on the photoemulsion because of the decrease of the effective aperture with increasing incident angle; (iv) the colour density curves of the colour reversal films (used as detectors) given by the producer; (v) the measured brightness and contrast transfer function of the scanner used for digitization of the colour slides of the sky. Characteristics (i)–(v) describe how the angular imaging, intensity, polarization, and spectral composition of the incident light are influenced by the optics and detector (photoemulsion) of the polarimeter and by the scanner (digitization). Although the responses of both photographic film and scanner were nonlinear, this was taken into account because the transfer function between the digital brightness values and the density values of photoemulsion was measured, from which the incident light intensity was calculated using the density–exposure characteristic curves of the film (given by the producer). Since further details of our instrument are not appropriate for this article in this journal, a complete instrument analysis and description of our full-sky imaging polarimeter will be published elsewhere.

Fig. 2. Temporal change of the celestial pattern of the brightness (A), degree of polarization δ (B) and ***E***-vector alignment α with respect to the local meridian (C) measured in the blue spectral range (Table 3) in Kecel, Hungary during the total solar eclipse on 11 August 1999. Values of time and percent geometric obscuration of the sun's disk are given above every column. (D-G) Differences between the subsequent polarization patterns calculated for the entire sky apart from the overexposed areas and the landmarks/vegetation near the horizon. (D) Difference of the patterns of the degree of polarization. (E) Difference of the patterns of the ***E***-vector alignment. (F,G) Frequency (measured in arbitrary unit) of the degree of polarization difference $\Delta\delta$ and the ***E***-vector alignment difference $\Delta\alpha$. Overexposed areas of the sky and the landmarks/vegetation near the horizon are shaded by black in rows B-E. Bottom insets: points of the compass with the direction of the umbra's path; grey codes of the numerical values of δ, α, $\Delta\delta$ and $\Delta\alpha$. The black and white photographs of the sky in row A do not represent correctly the real brightness of the skylight, because they were taken with different times of exposure and apertures (see Table 2).

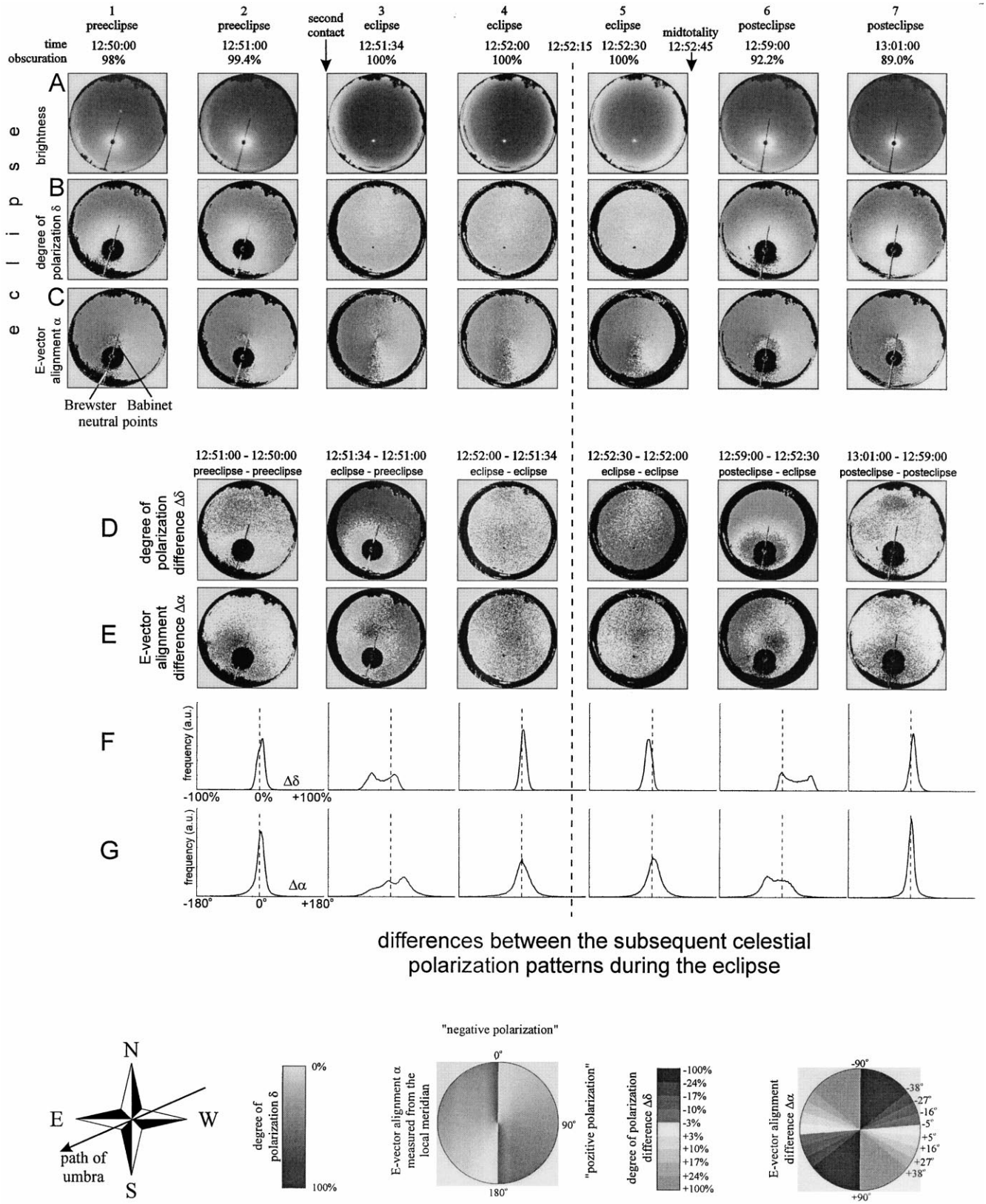
1 preeclipse
2 preeclipse
second contact
3 eclipse
4 eclipse
5 eclipse
midtotality
6 posteclipse
7 posteclipse
time
obscuration
12:50:00
98%
12:51:00
99.4%
12:51:34
100%
12:52:00
100%
12:52:15
12:52:30
100%
12:52:45
12:59:00
92.2%
13:01:00
89.0%
eclipse
A brightness
B degree of polarization δ
C E-vector alignment α
Brewster
Babinet
neutral points
12:51:00 - 12:50:00
preeclipse - preeclipse
12:51:34 - 12:51:00
eclipse - preeclipse
12:52:00 - 12:51:34
eclipse - eclipse
12:52:30 - 12:52:00
eclipse - eclipse
12:59:00 - 12:52:30
posteclipse - eclipse
13:01:00 - 12:59:00
posteclipse - posteclipse
D degree of polarization difference Δδ
E E-vector alignment difference Δα
F
frequency (a.u.)
Δδ
-100%
0%
+100%
G
frequency (a.u.)
Δα
-180°
0°
+180°
differences between the subsequent celestial polarization patterns during the eclipse
N
E
W
S
path of umbra
degree of polarization δ
0%
100%
"negative polarization"
E-vector alignment α measured from the local meridian
0°
90°
180°
"pozitive polarization"
degree of polarization difference Δδ
-100%
-24%
-17%
-10%
-3%
+3%
+10%
+17%
+24%
+100%
E-vector alignment difference Δα
-90°
-38°
-27°
-16°
-5°
+5°
+16°
+27°
+38°
+90°

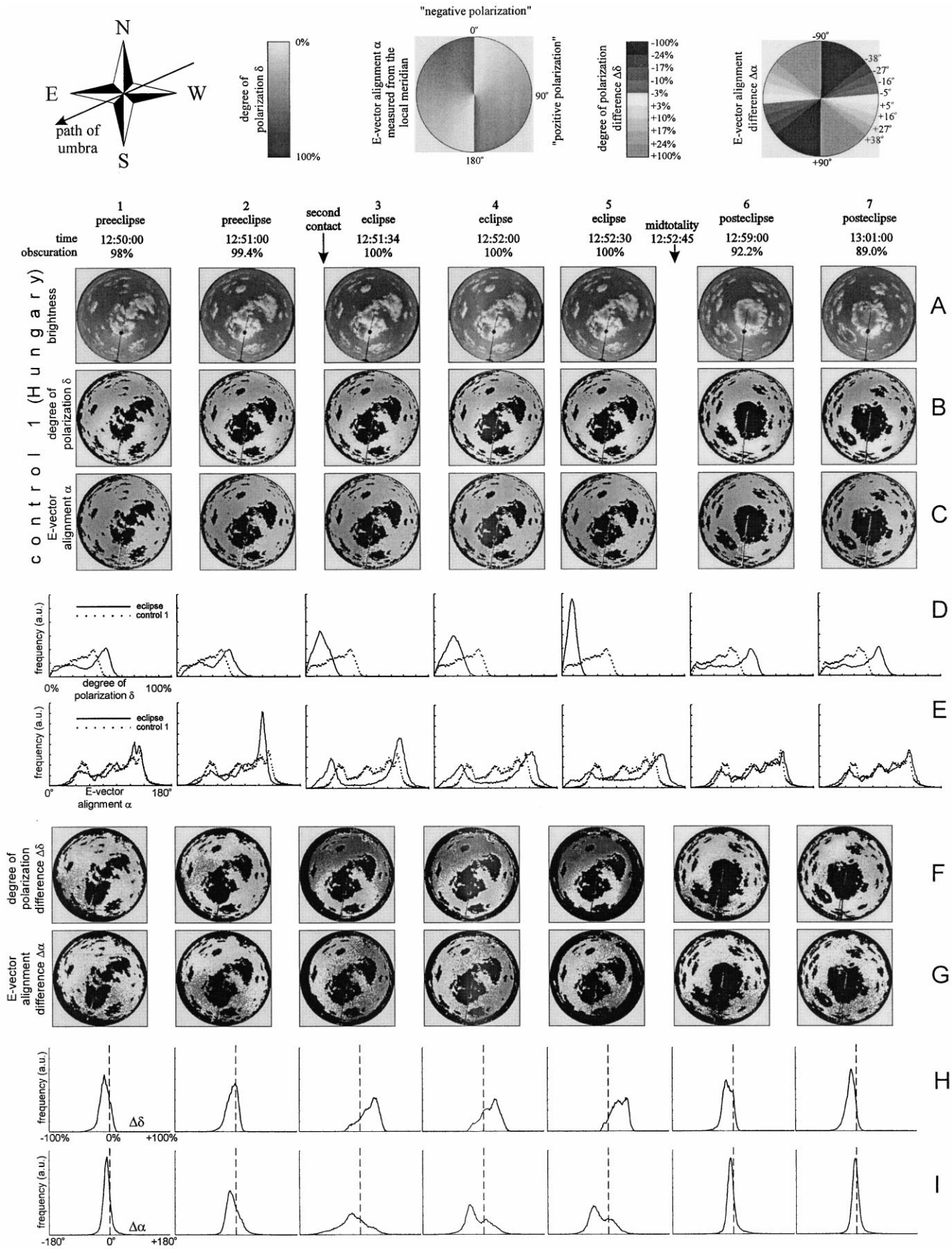
N
E
W
S
path of umbra
degree of polarization δ
0%
100%
"negative polarization"
E-vector alignment α measured from the local meridian
0°
90°
180°
"pozitive polarization"
degree of polarization difference Δδ
-100%
-24%
-17%
-10%
-3%
+3%
+10%
+17%
+24%
+100%
E-vector alignment difference Δα
-90°
-38°
-27°
-16°
-5°
+5°
+16°
+27°
+38°
+90°
1 preeclipse
2 preeclipse
second contact
3 eclipse
4 eclipse
5 eclipse
midtotality
6 posteclipse
7 posteclipse
time
12:50:00
12:51:00
12:51:34
12:52:00
12:52:30
12:52:45
12:59:00
13:01:00
obscuration
98%
99.4%
100%
100%
100%
92.2%
89.0%
control 1 (Hungary)
brightness
degree of polarization δ
E-vector alignment α
A
B
C
eclipse
control 1
frequency (a.u.)
degree of polarization δ
0%
100%
D
E-vector alignment α
0°
180°
E
degree of polarization difference Δδ
F
E-vector alignment difference Δα
G
Δδ
-100%
0%
+100%
H
Δα
-180°
0°
+180°
I
difference = control 1 - eclipse

2.3. Algorithmic recognition of colourless clouds and overexposed areas in the sky, and underexposed landmarks and vegetation near the horizon

The clouds were recognized in the digitized pictures of the sky by the use of the following simple algorithm: The light intensities I_r, I_g, I_b of every pixel of the picture measured in the red, green, and blue spectral range (Table 3) were compared with each other. If the differences $\Delta I_{b\text{-}r} = |I_b - I_r|$ and $\Delta I_{b\text{-}g} = |I_b - I_g|$ were smaller than $\epsilon = cI_b$ (c = constant), then it was assumed that the given pixel belonged to a cloud, else, to the clear blue sky. The essence of this algorithm is that, at smaller solar zenith distances θ_s (which was about 32° during the Hungarian eclipse), the clouds are generally colourless (ranging from dark grey to bright white), independent of their brightness and position in the sky, i.e., the pixels of clouds possess approximately the same light intensities in all three (r, g, b) spectral ranges. Setting appropriately the value of constant c, we could reliably recognize the clouds in the sky.

In certain regions (around the sun during the partial eclipse and in the control skies, and near the horizon during totality), the photoemulsion became inevitably overexposed or underexposed. These colourless (white or black) regions were recognized in the evaluation process (in the derivation of the polarization parameters) by the same algorithm as the colourless clouds.

In certain sky pictures, landmarks and vegetation were seen near the horizon. Since these areas were always underexposed (dark grey) on the photoemulsion, they could be recognized by the following simple algorithm: If the I_r, I_g, I_b values of a pixel were smaller than a given threshold t and $|I_b - I_g|$, $|I_b - I_r|$ were smaller than $t/2$, then it was assumed that the given pixel belonged to landmarks or vegetation. Setting appropriately the value of t, the landmarks and vegetation could be reliably recognized near the horizon.

2.4. Calculation of single-scattering Rayleigh skylight

The three-dimensional celestial hemisphere was represented in two dimensions by a polar coordinate system, where the angular distance θ from the zenith and φ from the solar meridian are measured radially and tangentially, respectively. In this two-dimensional coordinate system, the zenith is at the origin, and the horizon corresponds to the outermost circle. The theoretical polarization of the sky was described by the single-scattering Rayleigh model (Coulson, 1988).

In the single-scattering Rayleigh atmosphere, the degree of linear polarization of skylight is expressed by the formula $\delta = \delta_{max}\sin^2\gamma/(1+\cos^2\gamma)$, $\cos\gamma = \sin\theta_s\sin\theta\cos\varphi + \cos\theta_s\cos\theta$, where γ is the angular distance between the observed celestial point and the sun, θ and φ are the angular distances of the observed point from the zenith and the solar meridian, respectively. In the single-scattering Rayleigh model, the maximum degree of polarization amounts to $\delta_{max} = 100\%$. However, a number of atmospheric perturbatory effects (e.g., multiple scattering, ground reflection, presence of dust and molecular anisotropies) cause more or less deviations from the ideal Rayleigh model. One can partly take into consideration these effects using an empirical relationship between δ_{max} and the zenith distance θ_s of the sun. For a given θ_s, δ_{max} was determined from the patterns of the degree of polarization of normal (control) skylight measured by 180° field-of-view imaging polarimetry.

At any point in the single-scattering Rayleigh atmosphere, the ***E***-vector alignment is perpendicular to the plane of the triangle formed by the sun, the observer, and the point observed. So the ***E***-vector can be characterized by the unity vector $\boldsymbol{e} = \boldsymbol{v}\cos\alpha + \boldsymbol{h}\sin\alpha$, $\boldsymbol{v} = (-\cos\theta\cos\varphi, -\cos\theta\sin\varphi, \sin\theta)$, $\boldsymbol{h} = (-\sin\varphi, \cos\varphi, 0)$ in the point $(1,\theta,\varphi)$ of the spherical coordinate system representing the firmament, where α is the direction of ***E***-vector measured from the local meridian of the point observed. Using spherical geometry, α can be expressed as $\alpha = \arctan[(\sin\theta\cos\theta_s - \cos\theta\cos\varphi\sin\theta_s)/(\sin\varphi\sin\theta_s)]$.

3. Results

3.1. Temporal change of the celestial polarization pattern during the eclipse

Although we measured the celestial polarization patterns from the beginning (first contact, 11:28:35) to the end (fourth contact, 14:15:35) of the partial eclipse, we present here only the patterns from 12:50:00 (pre-eclipse, 98% obscuration) to 13:01:00 (posteclipse, 89% obscuration) because practically only in this time interval did detectable differences in the degree of polarization and ***E***-vector alignment of skylight in comparison with the normal (control) skylight occur.

Fig. 3. Temporal change of the normal celestial pattern of the brightness (A), degree of polarization δ (B), and ***E***-vector alignment α (C) measured in the blue spectral range (Table 3) in Kecel (Hungary) on 12.08.1999 as Control 1. The sky patterns recorded at 12:51:00 on 12.08.1999 were used as Control 1 for all the sky patterns recorded at 12:51:00, 12:51:34, 12:52:00, and 12:52:30 on 11.08.1999. (D, E) Frequencies of δ and α calculated for the entire sky apart from clouds, overexposed areas, and landmarks/vegetation on 11.08.1999 (eclipse) and 12.08.1999 (Control 1). (F–I) Differences between the polarization patterns apart from the clouds, overexposed areas, and landmarks/vegetation measured on 11.08.1999 (eclipse) and 12.08.1999 (Control 1) in Kecel. (F) Difference of the degree of polarization patterns. (G) Difference of the ***E***-vector alignment patterns. (H, I) Frequencies of $\Delta\delta$ and $\Delta\alpha$. All differences were formed in such a way that the eclipse values were subtracted from the control values. Overexposed and cloudy areas of the sky and the landmarks/vegetation near the horizon are shaded by black in rows B, C, F, G.

Fig. 2A–C shows the temporal change of the celestial pattern of brightness, degree of polarization, and ***E***-vector alignment measured in the blue spectral range (Table 3) in Kecel (Hungary) during the total solar eclipse on 11 August 1999. The values of time and percent geometric obscuration of the sun's disk are given in every column. During the totality, we were able to measure the sky polarization pattern at three different times prior to the midtotality (12:52:45): The first recording was taken at 12:51:34 (at the moment of the second contact); the second and third ones, at 12:52:00 and 12:52:30. In the area around the sun (during totality, only the solar corona) and near the horizon, the photoemulsion was overexposed. Such overexposure could be eliminated only by decreasing the time of exposure, but then, other regions of the photoemulsion would be underexposed. During the evaluation of the polarization of skylight, our computer program recognized these overexposed regions, which were not taken into consideration in the further calculations.

From Fig. 2B,C it is evident that the celestial polarization pattern suffers a sudden and dramatic change at the moment of the beginning and the end of the total eclipse. Immediately prior to and after the totality, the qualitative characteristics of the polarization pattern of the sky are very similar to those of the normal sky (Figs. 3, 4, and 8E,F): Apart from the region around the sun — where the Babinet and Brewster neutral points of skylight polarization occur (Coulson, 1988; Horváth et al., 1998) — (1) the degree of polarization of skylight gradually increases with increasing angular distance from the sun it reaches a maximum value at 90° from the sun, then it decreases towards the antisun; and (2) the ***E***-vector alignment of skylight is approximately tangential with respect to the sun, i.e., it is approximately perpendicular to the plane determined by the sun, the observer, and the celestial point observed. Apart from the regions around the neutral points, these celestial polarization patterns resemble the corresponding theoretical patterns computed on the basis of the single-scattering Rayleigh model (Fig. 8E,F).

During totality, however, the distribution of the degree of polarization δ of skylight becomes roughly cylindrically symmetric with respect to the zenith (Fig. 2B3–B5). The value of δ gradually increases from the horizon, then reaching a maximum, it gradually decreases towards the zenith, where it is approximately zero. During totality, the distribution of the ***E***-vector alignment of skylight remains asymmetric with respect to the zenith (Fig. 2C3–C5). But comparing with the pre-eclipse (Fig. 2C1,C2) and posteclipse (Fig. 2C6,C7) ***E***-vector patterns during totality, the region of "negative polarization" (shaded with dark grey or bright grey in row C of Fig. 2, where the angle α of the ***E***-vectors falls within the range of $-45° \le \alpha \le +45°$ with respect to the local meridian) considerably extends at cost of the area of "positive polarization" (shaded by middle grey in row C of Fig. 2, where $45° < \alpha < 135°$).

Fig. 2D,E shows the differences between the subsequent polarization patterns in Fig. 2B and C, respectively, calculated for the entire sky apart from the overexposed areas and landmarks/vegetation. Bright grey shades represent degree of polarization differences $+3\% \le \Delta\delta \le +100\%$, while dark grey shades indicate $-100\% \le \Delta\delta < -3\%$. The change of δ was not greater than $\pm 24\%$ within a few minutes, immediately prior to and after the totality (Fig. 2D2,D7). The same was true for the period of the total eclipse (Fig. 2D4,D5). After the second (Fig. 2D3) and third (Fig. 2D6) contacts, however, on a considerable area of the sky (for angular distances from the sun greater than about 55°), $|\Delta\delta| > 24\%$ differences occurred.

We can see that the sign of $\Delta\delta$ was approximately mirror-symmetrical to the time of about 12:52:15 in patterns D3–D6 in Fig. 2, where positive or negative $\Delta\delta$ values occur in patterns D3 and D4; there, negative or positive $\Delta\delta$ values occur in patterns D5 and D6, respectively. This can be explained in the following way: From the first contact to about 12:52:15, the deviations of skylight polarization from the normal celestial polarization gradually increased. From ca. 12:52:15 to the fourth contact, however, the sign of these deviations reverted, and their absolute value gradually decreased. Thus, the skylight polarization reverted to its normal state after 12:52:15.

The change of the pattern of the ***E***-vector alignment α of skylight, seen in Fig. 2E, was qualitatively similar to that of δ: The α pattern suddenly changed at the moment of the second (Fig. 2E3) and third (Fig. 2E6) contacts; otherwise, its change was rather modest (Fig. 2E2,E4,E5,E7); the sign of $\Delta\alpha$ was again more or less mirror-symmetrical to 12:52:15 (Fig. 2E3–E6). For zenith distances greater than about 20°, the values of $|\Delta\alpha|$ were smaller than 38°. Greater changes of α than $\pm 38°$ occurred only around the zenith at the second (Fig. 2E3) and third (Fig. 2E6) contacts.

Fig. 2F,G shows the frequencies of $\Delta\delta$ and $\Delta\alpha$ calculated for the entire sky apart from the overexposed areas and landmarks/vegetation. In these diagrams, small or great polarization differences are characterized by narrow or wide distribution functions, respectively, around the zero difference marked by a vertical broken line. Here we can see again how relatively small was the change of skylight polarization during the pre-eclipse (Fig. 2F2,G2), eclipse (Fig. 2F4,F5,G4,G5), and posteclipse (Fig. 2F7,G7) periods, and how great changes occurred in the state of skylight polarization at the moment of the second (Fig. 2F3,G3) and third (Fig. 2F6,G6) contacts. The distribution functions of $\Delta\delta$ and $\Delta\alpha$ possess two peaks at the second and third contacts: One of these peaks is placed in the positive range and the other peak in the negative range. The maximal value of $|\Delta\delta|$ was about 55%. The approximate mirror symmetry

Fig. 4. As Fig. 3 measured in the Chott el Djerid, 10 km from Kriz, Tunisia, on 26 August 1999 as Control 2.

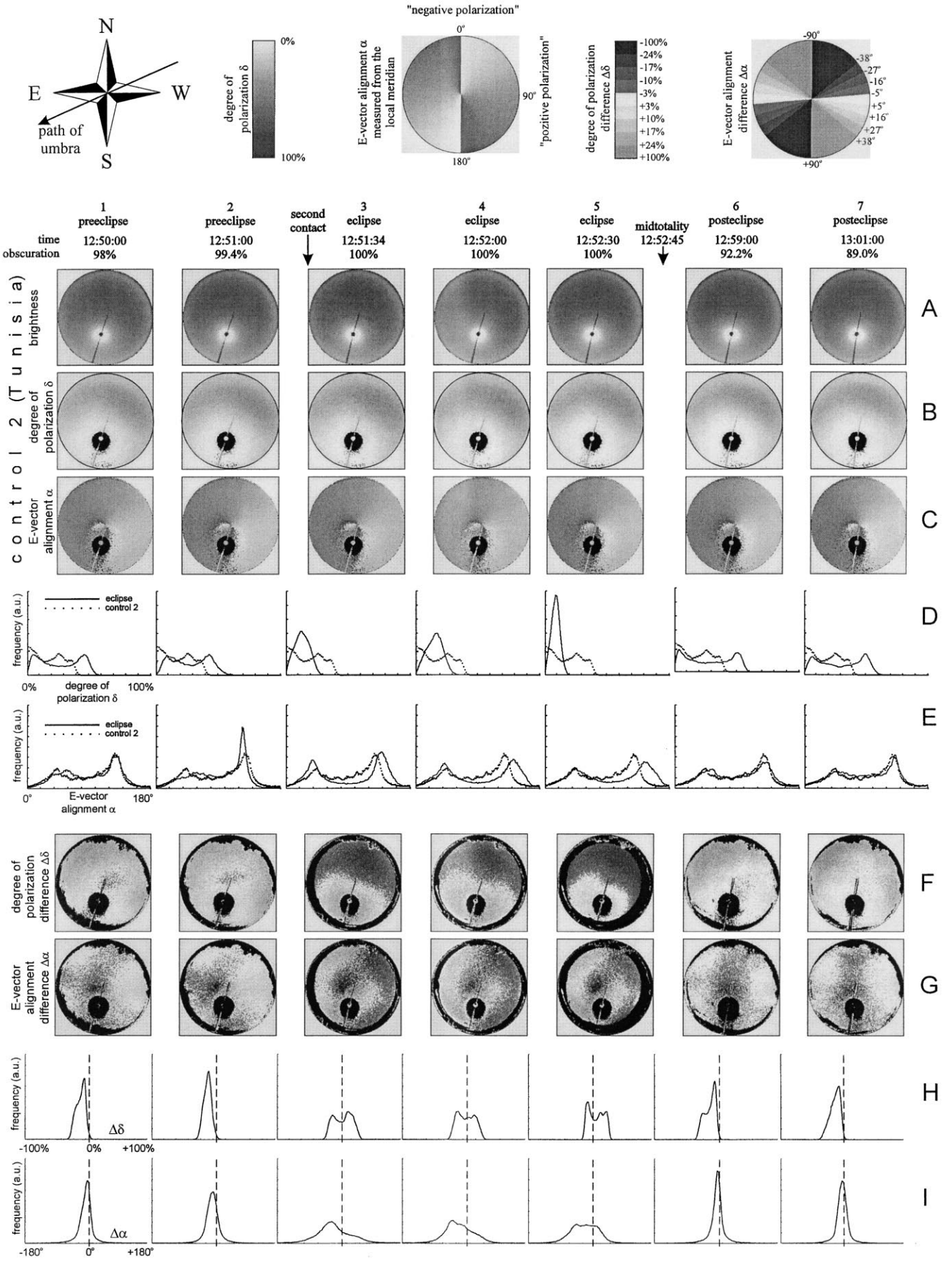
N
E
W
S
path of umbra
degree of polarization δ
0%
100%
"negative polarization"
E-vector alignment α measured from the local meridian
0°
90°
180°
"pozitive polarization"
degree of polarization difference Δδ
-100%
-24%
-17%
-10%
-3%
+3%
+10%
+17%
+24%
+100%
E-vector alignment difference Δα
-90°
-38°
-27°
-16°
-5°
+5°
+16°
+27°
+38°
+90°
1 preeclipse
2 preeclipse
second contact
3 eclipse
4 eclipse
5 eclipse
midtotality
6 posteclipse
7 posteclipse
time
12:50:00
12:51:00
12:51:34
12:52:00
12:52:30
12:52:45
12:59:00
13:01:00
obscuration
98%
99.4%
100%
100%
100%
92.2%
89.0%
control 2 (Tunisia)
brightness
degree of polarization δ
E-vector alignment α
A
B
C
eclipse
control 2
frequency (a.u.)
0%
degree of polarization δ
100%
D
0°
E-vector alignment α
180°
E
degree of polarization difference Δδ
F
E-vector alignment difference Δα
G
Δδ
-100%
0%
+100%
H
Δα
-180°
0°
+180°
I
difference = control 2 - eclipse

of the distribution functions to 12:52:15 can be seen in Fig. 2F,G, too.

Fig. 5B,C shows the spatial change of the degree of polarization δ and ***E***-vector alignment α of skylight as a function of time along four differently oriented meridians of the Hungarian eclipse skies measured in the blue spectral range (Table 3). The meridian marked with a square is perpendicular, and the meridian marked with a triangle is approximately parallel to the solar/antisolar meridian; the angle of the meridians marked with + and $\times$ is 45° and 135°, respectively, with respect to the antisolar meridian (Fig. 5E,F). The meridian marked with a triangle is not exactly parallel to the solar meridian because the latter was occluded by the wire holding the small disk, which screened out the sun during the control measurements.

We can see in Fig. 5B1,B2,B6,B7 that during the preeclipse and posteclipse periods, the celestial distribution of δ was not rotationally symmetric: In the antisolar hemisphere of the sky, always higher δ values occurred than in the solar hemisphere. At the second contact, the pattern of δ became approximately rotationally symmetric, a feature which remained throughout the totality, as can be seen in Fig. 5B3–B5, especially in Fig. 5B5. The celestial distribution of δ was, however, not exactly cylindrically symmetric to the zenith during totality. Smaller deviations from the rotational symmetry occurred especially along the meridian marked with a triangle (Fig. 5B3,B4).

The change of α along the different meridians of the sky was rather complex (Fig. 5C), but it can be clearly seen that the change of α along all meridians during totality (Fig. 5C3–C5) was substantially different from that during the preeclipse (Fig. 5C1,C2) and posteclipse (Fig. 5C6,C7) periods.

Figs. 2A3–A5 and 5E demonstrate that although the distribution of the brightness of skylight during totality was remarkably smooth and tended to be approximately symmetrical around the zenith, the same cannot be said for the distribution of the ***E***-vector alignment of skylight (Figs. 2C3–C5 and 5C3–C5). On the other hand, there is no tendency for the normal degree of polarization field to be symmetrical about the zenith (Figs. 3B, 4B, 5A, and 8E), in distinct contrast to the approximately symmetrical distribution of δ observed during totality (Figs. 2B3–B5, 5B3–B5, and 7G).

Earlier investigators of total eclipses could measure the skylight polarization averaged only in relatively small windows of the sky (generally at the zenith, or at 90° from the sun on the antisolar meridian, or at the cross-section of the almucantar and the solar and antisolar meridians, or perpendicularly to the solar meridian) because they had point-source polarimeters with a field of view of a few degrees. In order to compare our results with the observations of earlier authors, in Fig. 6, we plotted the temporal change of the degree of polarization δ and ***E***-vector alignment α of skylight measured in the blue spectral range (Table 3) within four different small celestial windows with a field of view of about $5° \times 5°$. The four windows designated by A, B, C, and D are represented in the bottom right inset of Fig. 6 and correspond with the windows generally chosen by earlier authors.

In windows A and B, δ considerably decreased during totality, while it varied only slightly in windows C and D. The variation of α was relatively small in window A, it was greater in windows B and D, while α suffered a considerable change in window C. Considering the temporal variation of δ and α at the beginning and the end of totality, we can see in Fig. 6 that all possible combinations could be observed in the sky: (1) remarkable changes of δ associated with almost no change of α in window A; (2) considerable changes of δ associated with moderate variations of α in window B; (3) small variations of δ associated with considerable changes of α in window C; (4) small variations of δ associated with modest variations of α in window D.

This high diversity of the changes of δ and α of skylight is the consequence of the spatiotemporal complexity of the celestial polarization pattern observed during the total eclipse (Fig. 2). Fig. 6 demonstrates well how strongly dependent is the temporal change of δ and α on the direction of view in the sky. Due to this strong dependence, the interpretation and comparison of observations on the temporal change of skylight polarization during total eclipses are difficult and problematic if the observations by different authors were performed at different angles of view in the sky.

We can see in Figs. 2, 5, and 6 that as the umbra moved across the observation point, the sky polarization varied somewhat during totality due to the change of scattering geometry.

3.2. Comparison with the polarization patterns of normal control skies

In order to compare the polarization patterns of skylight observed during the total eclipse of 11 August 1999 with the normal celestial polarization patterns, we measured the latter on 12 August 1999 in Kecel at the same place and times as on 11 August 1999. This series of normal celestial polarization patterns served as "Control 1." Since the sky was

Fig. 5. Spatial change of the degree of polarization δ (A, B) and ***E***-vector alignment α measured from the local meridian (C, D) of skylight as a function of time (1–7) along four differently oriented meridians (coded with $\times$, square, +, and triangle in figures E and F) of the Hungarian eclipse skies (B, C) and the Tunisian control skies (A, D) measured in the blue spectral range (Table 3). The shape of the data points in the diagrams coincides with the shape of the symbols coding the different meridians indicated in figures E and F. Every data point represents a value averaged on δ or α values measured in 33 neighbouring celestial points along a given meridian. The position of the neutral point near the zenith occurring during the totality is marked by a vertical broken line in diagrams B3–5.

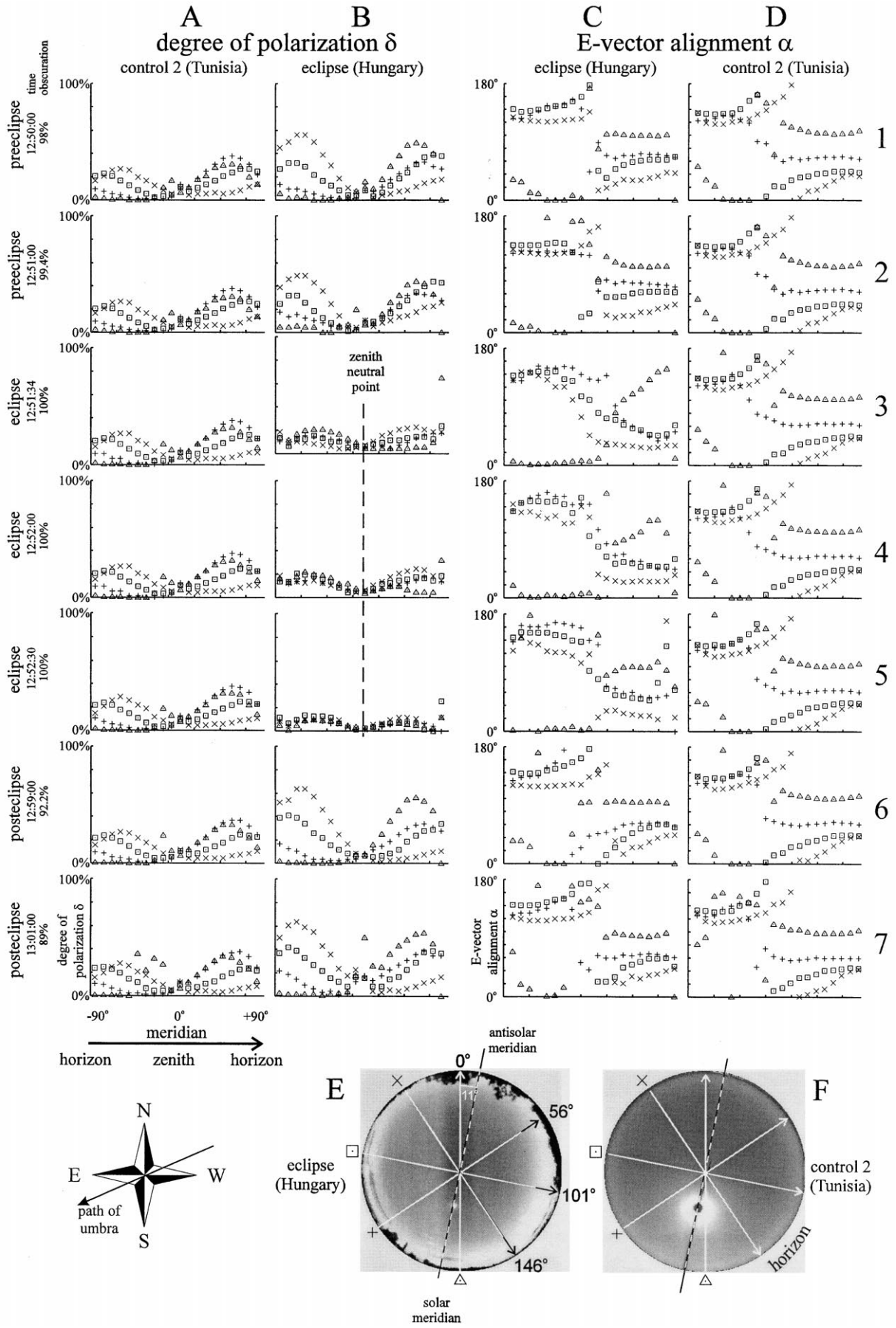
A
B
C
D
degree of polarization δ
E-vector alignment α
control 2 (Tunisia)
eclipse (Hungary)
eclipse (Hungary)
control 2 (Tunisia)
time
obscuration
preeclipse 12:50:00 98%
preeclipse 12:51:00 99.4%
eclipse 12:51:34 100%
eclipse 12:52:00 100%
eclipse 12:52:30 100%
posteclipse 12:59:00 92.2%
posteclipse 13:01:00 89%
zenith neutral point
100%
0%
180°
0°
1
2
3
4
5
6
7
degree of polarization δ
E-vector alignment α
-90°
0°
+90°
meridian
horizon
zenith
horizon
N
E
W
S
path of umbra
E
F
antisolar meridian
0°
11°
56°
101°
146°
solar meridian
eclipse (Hungary)
control 2 (Tunisia)
horizon

partially cloudy on the Hungarian control day, we repeated the control measurement in the Chott el Djerid (10 km from Kriz, Tunisia) on 26 August 1999 for the same solar zenith distance of 32° as during the Hungarian total eclipse. The Tunisian series of normal, cloudless, celestial polarization patterns served as "Control 2." The results of these two control measurements are presented in Figs. 3 and 4 in the blue spectral range (Table 3).

Figs. 3D,E and 4D,E show the frequencies of δ and α calculated for the same common clear regions of the eclipse and control skies. Figs. 3F–I and 4F–I represent the differences between the eclipse and control polarization patterns. The differences were formed in such a way that the polarization values measured during the eclipse were subtracted from the polarization values measured during the control ($\Delta\delta = \delta_{control} - \delta_{eclipse}$, $\Delta\alpha = \alpha_{control} - \alpha_{eclipse}$). In the calculation of the frequencies of $\Delta\delta$ and $\Delta\alpha$, the union of the cloudy and overexposed areas of the sky and the landmarks/vegetation near the horizon were not taken into account (the number of pixels in the remaining clear and non-overexposed areas of the sky was about 70 000, which is 20% of the total number of 350 000).

We can see in Figs. 3 and 4 that in the last minutes of the pre-eclipse period and in the first minutes of the posteclipse period, the polarization patterns of skylight differed only slightly from the corresponding normal celestial polarization patterns. The relative degree of polarization differences were, however, always greater than the relative ***E***-vector alignment differences both during the pre-eclipse and posteclipse periods. Before 12:50:00 and after 12:59:00, i.e., when the percent geometric obscuration of the sun's disk was smaller than about 92–98%, there were practically no polarization differences between the eclipse and normal skies.

During the total eclipse, both δ and α of skylight differed significantly from those of normal skylight as can be seen in Figs. 3 and 4. During totality, δ considerably decreased in the antisolar hemisphere, where in a relatively great region of the sky, $\Delta\delta = \delta_{control} - \delta_{eclipse} > 24\%$ values occurred (Figs. 3F and 4F). On the other hand, during totality, δ increased in the solar hemisphere, where $\Delta\delta = \delta_{control} - \delta_{eclipse} < -24\%$ values occurred in the vicinity of the eclipsed sun. During the total eclipse, the most significant changes of α happened in and around the zenith, where, also, $|\Delta\alpha| = |\alpha_{control} - \alpha_{eclipse}| > 38°$ values occurred (Figs. 3G and 4G). During totality, in the sky westward from the solar/antisolar meridian, the sign of $\Delta\alpha$ was opposite of that eastward from the solar/antisolar meridian (Figs. 3G3–G5 and 4G3–G5).

Fig. 8E,F shows the normal celestial pattern of δ and α calculated on the basis of the single-scattering Rayleigh model for the same solar position as that of the eclipsed sun during the totality on 11 August 1999. Although the single-scattering Rayleigh sky is a gross approximation of the real sky, the Rayleigh patterns in Fig. 8E,F can serve as a relatively good reference for the corresponding measured skies in Figs. 2, 3, 4B,C.

In Fig. 5, we compare the spatial change of δ and α vs. time along four differently oriented meridians of the Hungarian eclipse skies and the Tunisian control skies measured in the blue spectral range (Table 3). We can see that during the pre-eclipse (rows 1 and 2 in Fig. 5) and posteclipse (rows 6 and 7 in Fig. 5) periods, the distribution (the shape of the graphs) of δ and α in the eclipse sky was qualitatively the same as that in the normal (Tunisian control) sky. Comparing the graphs in rows 3–5 of Fig. 5, we can see strikingly how the distribution of δ and α in the eclipse sky during totality differs from that in the normal sky.

(i) In the normal sky, the change of δ along all meridians is asymmetrical to the zenith during totality (Fig. 5A3–A5), while in the eclipse sky, it is approximately symmetrical to the zenith (Fig. 5B3–B5), which corresponds to a more or less cylindrically symmetric pattern of δ.

(ii) Although the change of α along every meridian is asymmetrical both in normal and eclipse skies, the shape of the graphs of α measured in the eclipse sky during totality (Fig. 5C3–C5) is substantially different from that observed in the normal sky (Fig. 5D3–D5).

(iii) During totality, the shape of the α graphs is more diffuse (Fig. 5C3–C5) at and near the zenith than in the case of the control skies (Fig. 5D3–D5). The reason for this is that at and around the zenith, the degree of polarization is very low (Fig. 5B3–B5); thus, the accuracy of the computation of the value of α is slightly reduced.

In Fig. 6, the temporal changes of δ and α observed within four different conventional windows of the Hungarian eclipse skies, Hungarian control skies, and Tunisian control skies measured in the blue spectral range (Table 3) are compared. We can see that both δ and α of both the Hungarian and Tunisian normal skylight varied only slightly and relatively smoothly vs. time in all four celestial windows during the 17 min from 12:45:00 to 13:02:00. During the pre-eclipse and posteclipse periods, the δ and α values of the eclipse skylight were near the values of the control skylight. Only in the zenith window C did significant differences between the α values of eclipse and normal skylight immediately prior to and after the totality occur. During totality, considerable changes of δ could be observed in windows A and B in comparison with the δ values of the normal skylight. The same was true for the change of α in window C. In other cases, there were small or moderate polarization differences between the windows in the eclipse and control skies.

3.3. Spectral characteristics of skylight polarization during totality

Fig. 7 shows the spectral characteristics of skylight polarization measured in the red, green, and blue spectral ranges (Table 3) during the total eclipse of 11 August 1999 at 12:52:30. The spectral characteristics of skylight were the same in the case of the other two times (12:51:34, 12:52:00)

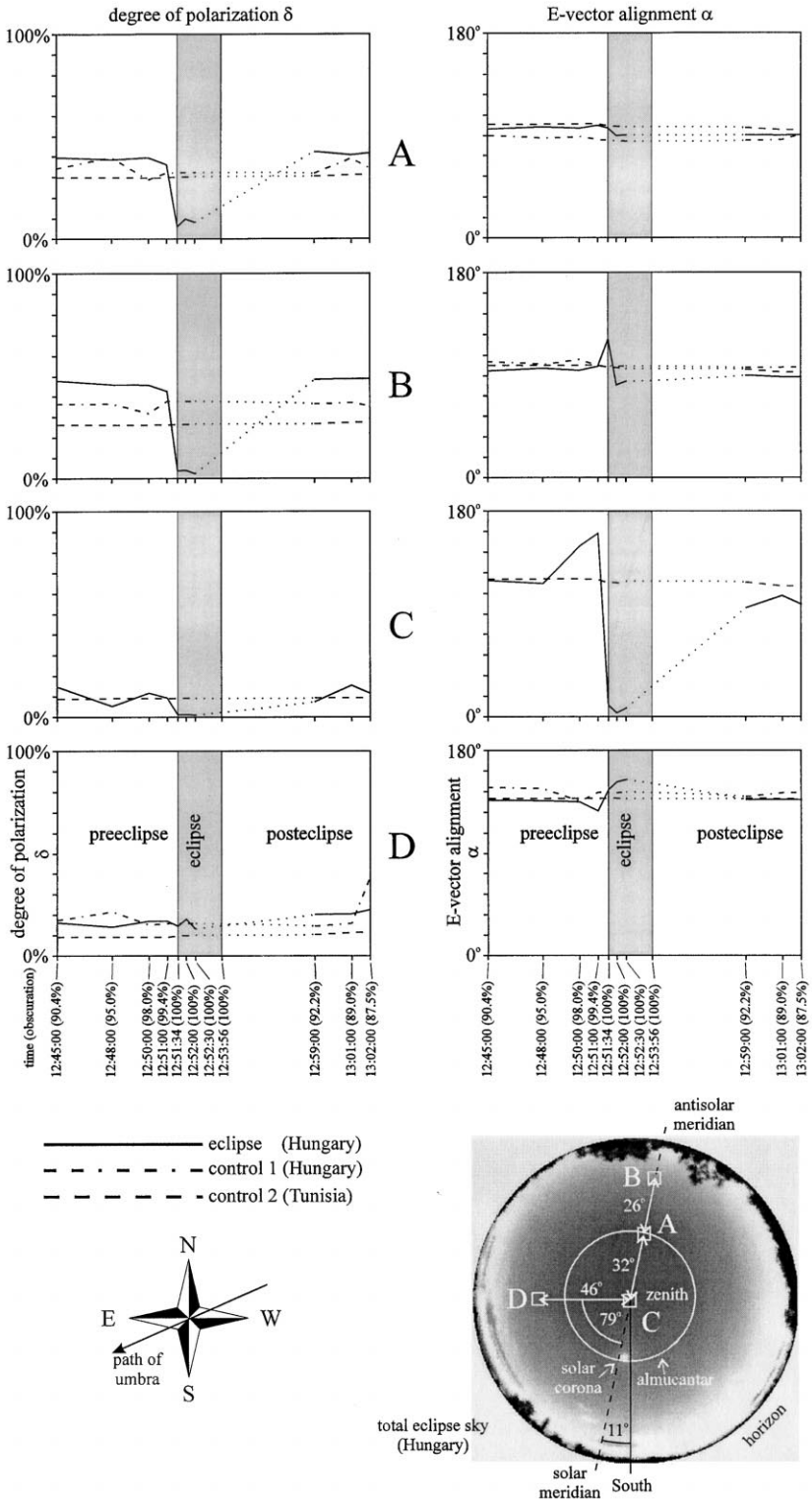

Fig. 6. Temporal change of the degree of polarization δ (left column) and ***E***-vector alignment α (right column) within four different windows (A–D) of the Hungarian eclipse skies (continuous line), Hungarian control skies (broken and dotted line), and Tunisian control skies (broken line) measured in the blue spectral range (Table 3). The diameter of the entire sky is 700 pixels, and the dimensions of the celestial windows are 20 × 20 pixels. (A) Window in the cross-section of the almucantar and the antisolar meridian positioned at the same angular zenith distance of 32° as the eclipsed sun. (B) Window on the antisolar meridian at 90° from the eclipsed sun. (C) Window at the zenith. (D) Window at an angle of 79° from the solar meridian with an angular zenith distance of 46°. Windows A, B, and D were cloudless during all measurements. The zenith window C was not always cloudless during the Hungarian control measurements; thus, Control 1 (broken and dotted line) was omitted for window C. The data points in the diagrams were simply connected with each other by straight lines (linear interpolation). The error bars were omitted for the sake of perspicuousness (the values of the standard deviation were not greater than 1–5% due to the small dimension of the celestial windows). The linear interpolation between the polarization values measured at 12:52:30 and 12:59:00 was represented by dotted lines in order to distinguish this relatively long time period (in which the photographic film was changed in the camera after the totality) from the others.

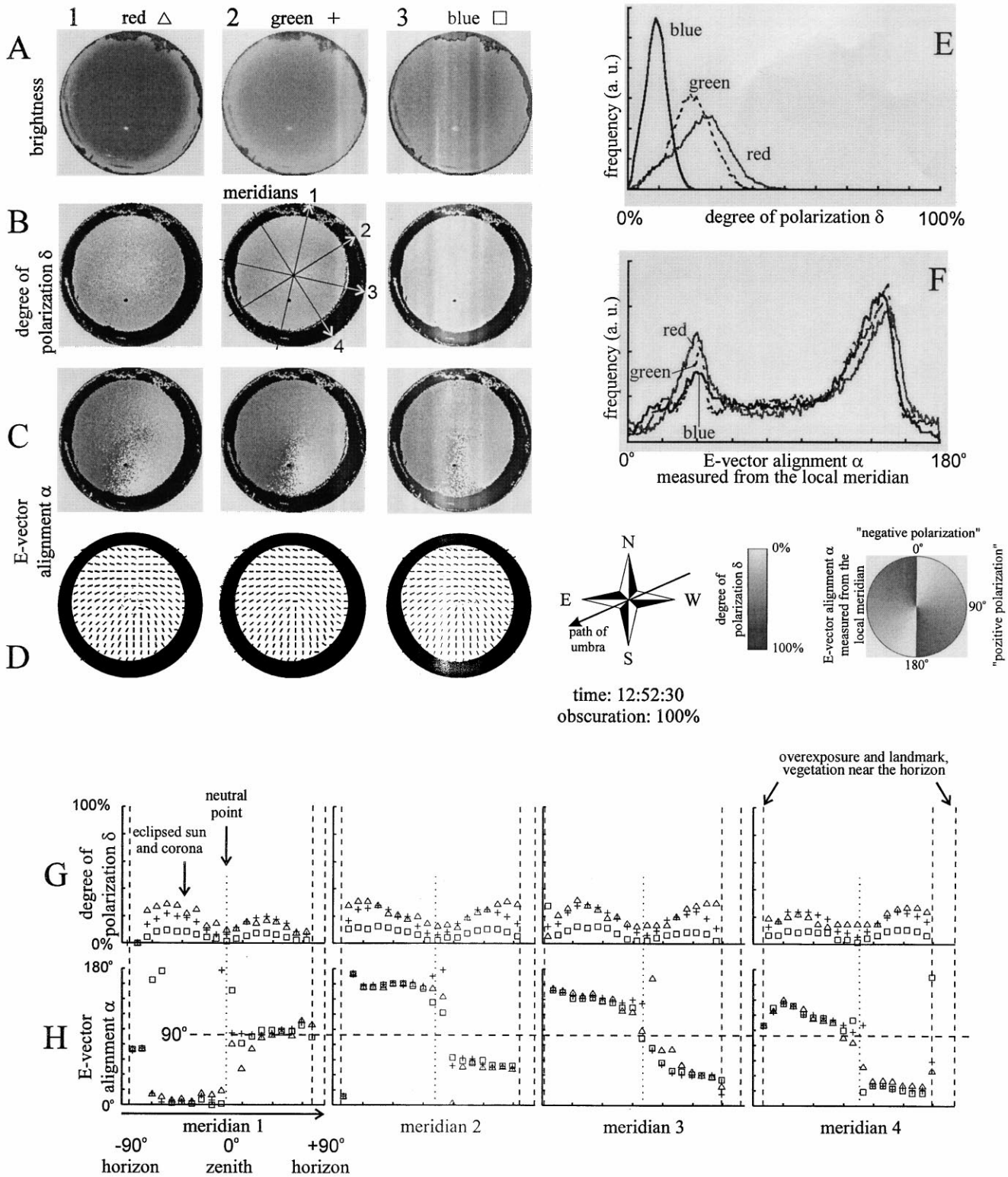

Fig. 7. Spectral characteristics of the brightness (A), degree of polarization δ (B, E, G), and ***E***-vector alignment α (C, D, F, H) of skylight measured in the red, green, and blue spectral range (Table 3) during the total eclipse of 11 August 1999 at 12:52:30. (A) Brightness patterns. (B) Patterns of δ. (C) Patterns of α. (D) Patterns of α, where the direction of the bars represents the local ***E***-vector alignment. (E, F) Frequencies of δ and α calculated for the entire sky apart from overexposed areas and landmarks/vegetation. (G, H) Spatial change of δ and α along four differently oriented meridians (designated by 1–4 in pattern B2) of the sky. The shape of the data points in diagrams G and H is a triangle, +, or square for the red, green, or blue spectral range, respectively. Every data point represents a value averaged on δ or α values measured in 33 neighbouring celestial points along a given meridian. The position of the neutral point is marked by a vertical dotted line in diagrams G, H. The areas of the sky with overexposure and landmarks/vegetation are shaded by black in rows B–D.

during totality. Apart from a reddish-orange, narrow annular zone at the horizon, during totality, the skylight was the brightest and the darkest in the blue and red range of the spectrum, respectively. These can be explained by the Rayleigh scattering, which results in higher intensities of scattered light for shorter wavelengths and higher intensities of "semidirect" light for longer wavelengths. During totality, "semidirect" light means the light that is scattered into the umbral area from the directly illuminated regions of the atmosphere outside the umbra.

Fig. 7B,E,G shows that during totality, the longer the wavelength of skylight, the higher is its degree of polarization. The physical reasons of this phenomenon are explained qualitatively in the Discussion. This observation contradicts with certain earlier (erroneous) observations. Contrary to the relatively great dispersion of the degree of polarization of skylight, the wavelength dependence of the ***E***-vector alignment of skylight was rather modest during totality as can be seen in Fig. 7C,D,F,H.

3.4. Neutral point of skylight polarization near the zenith during totality

Figs. 2B3–B5, 5B3–B5, 6C, and 7B,G show that a neutral point of skylight polarization occurred near the zenith during totality. In a neutral point, the degree of polarization δ is zero, and farther away from this celestial point, the value of δ gradually increases. Crossing this neutral point, the ***E***-vector alignment α suffers a sudden change in $\Delta\alpha$ ($|\Delta\alpha| = 90°$ for the solar/antisolar meridian) as can be seen in Figs. 2C3–C5, 5C3–C5, 6C, and 7C,D,H. The well-known Arago, Babinet, and Brewster neutral points of skylight polarization possess similar characteristics (Coulson, 1988; Horváth et al., 1998).

4. Discussion

4.1. Origin of the E-vector pattern during totality

Let us consider the origin of the sudden change of the ***E***-vector alignment of skylight when the zenith is crossed along the solar/antisolar meridian observed during totality (Fig. 8C). This switch of the ***E***-vector alignment occurs at the border of the region of "positive polarization" (shaded by middle grey in Fig. 2C) and "negative polarization" (shaded by dark grey or bright grey in Fig. 2C). Fig. 8A represents schematically how the originally unpolarized sunlight illuminating the atmosphere reaches an observer after primary and higher-order scattering events during the totality. Light from a first-order scattering event (A) can reach the observer only at very small angles of view with respect to the horizon. At greater viewing angles, light can reach the observer only due to second (B_2) or higher-order scattering events. The observed celestial polarization is the result of these higher-order scattering events. The magnitude of the very scant direct light of the solar corona can be neglected in comparison with the intensity of the scattered light coming from outside the umbral region of the atmosphere.

As a first approximation, let us try to explain qualitatively the ***E***-vector alignment of skylight during totality solely on the basis of first (A, B_1)- and second (B_2)-order scattering events. First-order scattering would result in the well-known Rayleigh pattern of skylight polarization. This is a relatively good description of the celestial polarization pattern apart from the regions of the sky surrounding the Arago, Babinet, and Brewster neutral points, which are positioned along the solar and antisolar meridian not farther away from the sun and antisun than about 25–30° (Coulson, 1988; Horváth et al., 1998). In Fig. 8B,D, the theoretical single-scattering Rayleigh pattern calculated for a solar zenith distance of 32° (corresponding with the solar zenith distance during totality on 11 August 1999 in Kecel, Hungary) can be seen. In the Rayleigh pattern, the bars represent the directions of the ***E***-vector of skylight and the length of the bars is proportional to the degree of polarization of skylight. The grey ellipse represents schematically the umbra during totality in the celestial hemisphere.

In our model during totality, the atmosphere is illuminated only by the single-scattering Rayleigh skylight from outside the umbral region. The atmospheric scattering centres (B_2) in the umbra scatter the rays of this Rayleigh skylight towards the observer (Fig. 8A). If the observer views towards the antisolar hemisphere of the umbra (Fig. 8B), this region of the atmosphere is illuminated mainly by highly polarized scattered Rayleigh skylight (B_1), the ***E***-vectors of which are approximately perpendicular to the scattering plane (the local meridian). This more or less perpendicularly polarized skylight is scattered (B_2) towards the observer. This is the reason behind the fact that during totality, we observed mainly "positive" (meaning, ***E***-vectors more or less normal to the scattering plane) skylight polarization (shaded by middle grey in Fig. 2C) in the antisolar hemisphere (top half of Fig. 8C).

If the observer views towards the solar hemisphere of the umbra (Fig. 8D), this region of the atmosphere is illuminated mainly by highly polarized scattered Rayleigh skylight (B_1), the ***E***-vectors of which are approximately parallel to the local meridian. This more or less parallelly polarized skylight is scattered (B_2) towards the observer. This is the reason behind the fact that during totality, we observed mainly "negative" (meaning, ***E***-vectors more or less parallel to the scattering plane) skylight polarization (shaded by dark grey or bright grey in Fig. 2C) in the solar hemisphere (bottom half of Fig. 8C). In Fig. 8C, we can see that the ***E***-vector alignment α suffers a sudden change when the zenith is crossed, and $|\Delta\alpha|$ is about 90° if we cross the zenith parallel to the solar/antisolar meridian.

Although during a total eclipse, higher than second-order scattering events also play an important role in the formation

of the celestial polarization pattern, the above simple qualitative derivation can explain the gross characteristics of the observed ***E***-vector pattern of skylight during totality surprisingly well.

4.2. Origin of the zenith neutral point during totality

Fig. 9 explains qualitatively the origin of the neutral (unpolarized) point of skylight polarization observed near

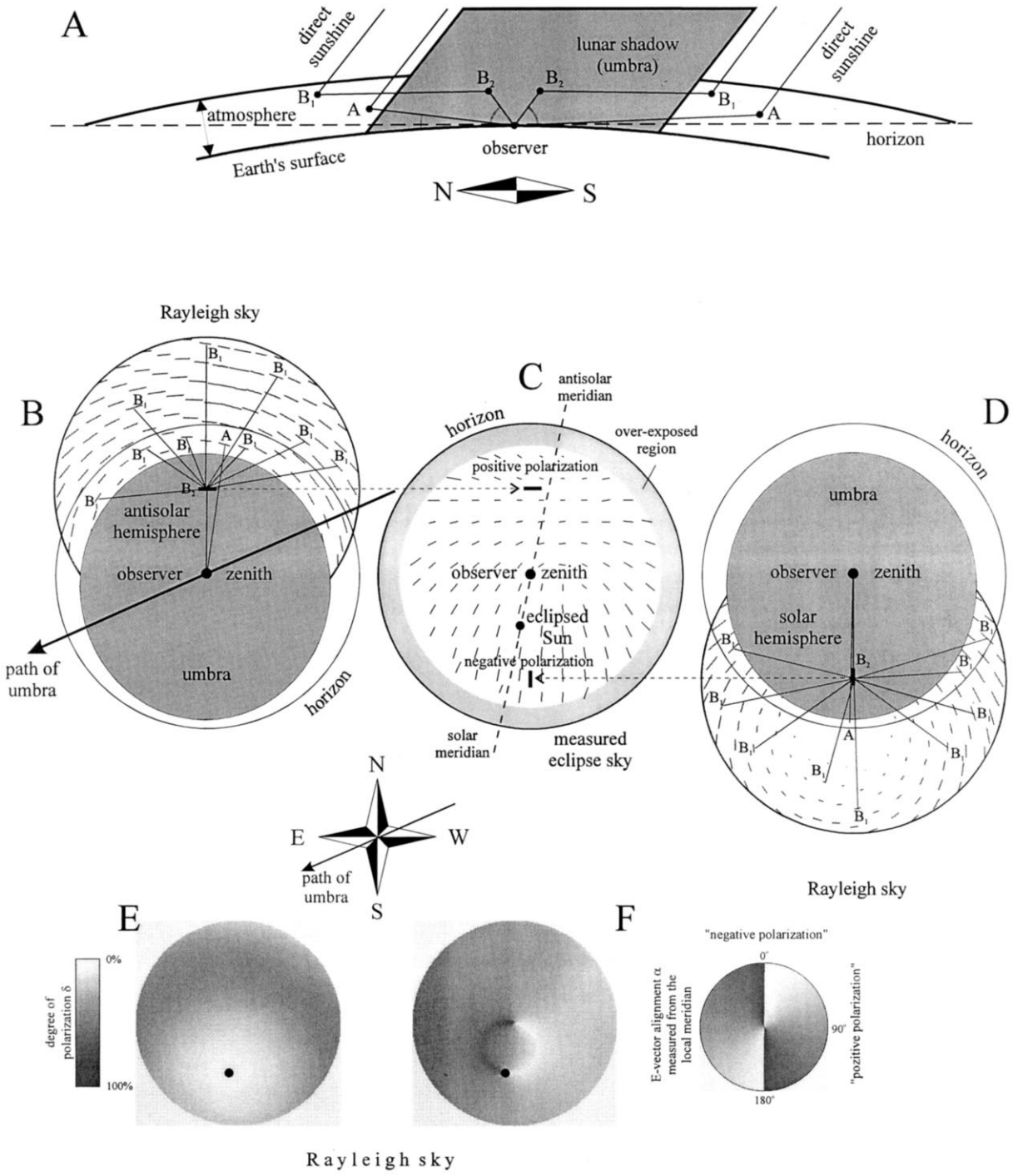

Fig. 8. (A) Schematic representation of the geometry of primary (A, B_1) and second-order (B_2) scattering of sunlight in the atmosphere during a total solar eclipse. (B–D) For the qualitative explanation of the origin of the region of "positive polarization" (B) and "negative polarization" (D) in the sky observed during totality. (E, F) The normal celestial patterns of the degree of polarization δ and ***E***-vector alignment α calculated on the basis of the single-scattering Rayleigh model for the same solar position as that of the eclipsed sun during the totality on 11 August 1999.

the zenith during totality. Our qualitative model is similar to that discussed in Section 4.1. If only primary (B_1) and second-order (B_2) scattering events are taken into account, the situation is as shown in Fig. 9A. Since the atmospheric scattering centres (B_2) at or near the zenith (above the observer in the umbra) are illuminated by single-scattered Rayleigh skylight with all possible directions of the ***E***-vector coming from outside the umbra (B_1), the atmosphere at or near the zenith scatters ***E***-vectors with all possible alignments towards the observer. This results in a zero net degree of polarization, i.e., unpolarized skylight near the zenith. If besides first (B_1)- and second (B_2)-order scattering, also third-order scattering events (B_3) are taken into account, the situation is as shown in Fig. 9B. In the umbra, from the northern (Fig. 9B4) or southern (Fig. 9B2) part of the sky (B_2), the atmospheric scattering centres (B_3) above the observer (at or near the zenith) are illuminated mainly by highly polarized scattered Rayleigh skylight (B_1), the ***E***-vectors of which are approximately perpendicular or parallel to the local meridian, respectively. From the western (Fig. 9B1) or eastern (Fig. 9B3) part of the sky (B_2), the atmospheric scattering centres at or near the zenith (B_3) are illuminated mainly by more or less polarized scattered Rayleigh skylight (B_1), the ***E***-vectors of which are more or less diagonal with respect to the local meridian. These, more or less, perpendicularly, parallelly, and diagonally polarized rays of skylight are scattered from the zenith (B_3) towards the observer (Fig. 9B5), resulting in all possible directions of the ***E***-vector. This results in, again, unpolarized (neutral) skylight at or near the zenith.

4.3. Relation to earlier observations on skylight polarization during total eclipses

4.3.1. Agreements with earlier eclipse observations

Let us consider the relation of our results to earlier total eclipse observations. de Bary et al. (1961) observed that the degree of polarization δ of skylight at 90° from the obscured sun reached zero at the time of totality on 15 February 1961 in Viareggio, Italy. The δ values remained low during totality. At 1 min before and after totality, the polarization was essentially normal, even though the light intensity reacted throughout the course of the eclipse. During totality, we observed very low, or even approximately zero, δ values near the horizon, at the zenith (where a neutral point occurred), as well as at about 90° from the obscured sun (Figs. 2B, 5B, 6, and 7). Similar to the eclipse observed by de Bary et al. (1961), on 11 August 1999, at Kecel, the skylight polarization pattern was essentially normal at a few (3–5) minutes before and after totality. These short periods represent a transition when multiply scattered light from outside the environs of the umbral zone becomes comparable in magnitude to the effects of the directly illuminating sunlight.

One would expect that the degree of polarization of skylight should diminish during totality because of the randomizing effects of multiple scattering. Indeed, as Figs. 2B, 3D, 4D, 5B, and 6 show, the degree of polarization of skylight did decrease as expected. This agrees reasonably well with other reported observations (e.g., Dandekar & Turtle, 1971; Moore & Rao, 1966; Rao, Takashima, & Moore, 1972).

Dandekar and Turtle (1971) observed that at a point 90° from the sun during the eclipse of 7 March 1970 in Kinston, USA, at totality, the planes of polarization changed by about 48° and 55° for 475 nm (blue) and 600 nm (red), respectively, with reference to that outside totality. At 90° from the obscured sun, we observed on 11 August 1999 at Kecel that at totality, the ***E***-vector alignment α changed by about $\Delta\alpha \approx \pm 20-25°$ (Fig. 6B). In certain other regions of the sky, also greater $\Delta\alpha$ values were observed (see Figs. 2C,E,G, 5, and 6); these were, however, not greater than about $\pm 38°$. Extremely great changes of $\Delta\alpha$ occurred only around the zenith (Figs. 2C,E,G, 5, and 6C). The magnitude of $\Delta\alpha$ at totality was approximately the same in the red, green, and blue spectral ranges (Table 3).

At totality, Moore and Rao (1966) did observe a change of 90° in the plane of polarization for blue ($\lambda = 400$ nm) skylight at the zenith. Their observation of no change of the plane of polarization for red ($\lambda = 600$ nm) skylight is, however, difficult to understand.

Shaw (1975), observing skylight at $\lambda = 400$ nm (blue) in the sun's vertical 90° from the sun during the 30 June 1973 total eclipse in Northern Kenya, found the degree of polarization to decrease from a pre-eclipse value of 45% to 4% during midtotality. The polarization decrease began 6–7 min before totality, and the depolarization effect disappeared in a like amount of time following totality. These observations are in qualitative agreement with our results.

Using a polarimeter oriented in the direction of the zenith and another polarimeter oriented at 90° from the sun in the sun's vertical, Coulson (1988) observed a virtual lack of polarization response during a partial (approximately 80%) eclipse of the sun at Davies, USA, on 26 February 1979. This was to be expected, as 20% of the unobscured solar disk results in the direct flux being greatly dominant over the diffuse flux.

Previous studies (e.g., Coulson, 1988; Sharp, Silverman, & Loyd, 1971) have indicated that up to approximately 98% geometric obscuration of the sun's disk eclipse phenomenology can be interpreted in terms of attenuated, but otherwise essentially unchanged, sunlight. For high obscuration ratios greater than about 98%, multiple scattering predominates, and the distribution of colour, intensity, and polarization over the sky hemisphere changes rapidly and dramatically. The degree of polarization tends to be rather symmetric about the zenith. Our observations are in accordance with these.

Hence, many details of our results are in agreement with several earlier eclipse observations. At this stage, a more

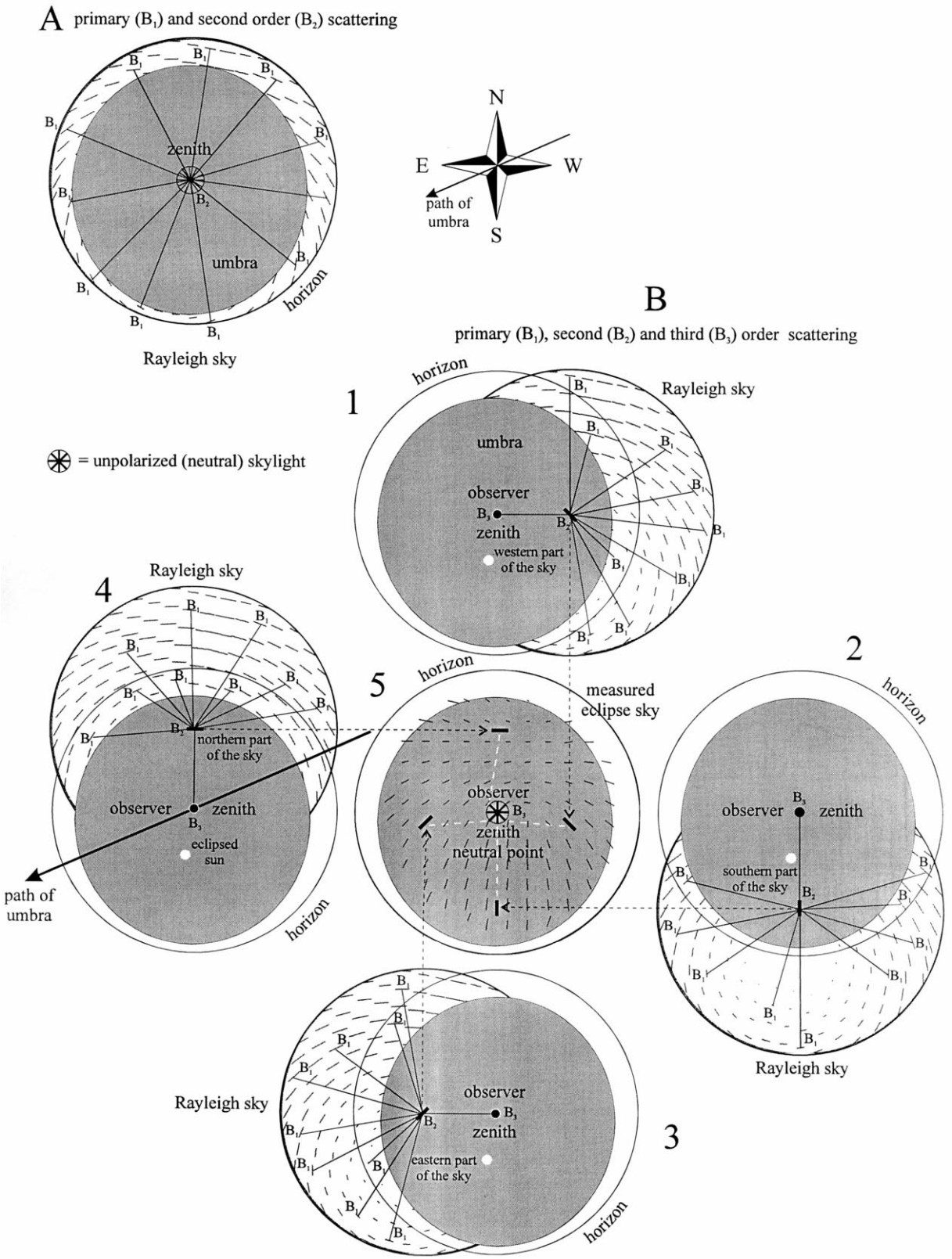

Fig. 9. For the qualitative explanation of the origin of the neutral (unpolarized) point of skylight polarization observed near the zenith during totality if primary and second-order scattering events (A), or first-, second-, and third-order scattering events (B) are taken into account.

detailed comparison is not possible because of a different geometry for each of these eclipses.

4.3.2. Disagreements with earlier eclipse observations

4.3.2.1. Spectral dependence of skylight polarization during totality. Under normal, clear atmospheric conditions, a general rule is that the shorter the wavelength, the lower the degree of polarization of multiply scattered skylight (Coulson, 1988; Subsection 5.2.3.3 Spectral Dependence of the Polarization, pp. 284–286, Figs. 5.5, 5.6). There is little spectral dependence at the longer wavelength range ($\lambda > 500$ nm), but strong dispersion for shorter wavelengths. The strong variation of the degree of polarization of skylight at shorter wavelengths is due mainly to multiple scattering because the degree of polarization resulting from a single-scattering event is essentially independent of wavelength.

The stronger the multiple scattering, the more the degree of polarization is reduced. Since the magnitude of multiple scattering increases as the wavelength of light decreases (due to Rayleigh scattering), at shorter wavelengths, multiple scattering reduces considerably the degree of polarization of skylight.

During a total solar eclipse, there is no direct illumination (apart from the scant light of the solar corona), and the umbral zone of the atmosphere is illuminated from outside the umbra predominantly by normal multiply scattered skylight, the degree of polarization of which is smaller at shorter wavelengths. This skylight suffers further multiple scattering in the umbral region of the atmosphere. The consequence of this is that the degree of polarization of skylight is further reduced by the umbral multiple scattering at all wavelengths. Since the magnitude of this umbral multiple scattering increases again with decreasing wavelength (i.e., the diffusion of blue light is more affected by multiple scattering processes than red light), at shorter wavelengths, the degree of polarization of skylight is much more reduced than at longer wavelengths. Hence, also a total eclipse is characterized by the general rule that the shorter the wavelength, the lower the degree of polarization of skylight, and there is a strong dispersion for shorter wavelengths.

Worthy of special note is that our observations are in agreement with the above theoretical considerations. In Fig. 7, we can see immediately that the longer the wavelength, the higher the degree of polarization of multiply scattered skylight during totality. This is the direct consequence of the theory of Rayleigh and multiple scattering (Chandrasekhar, 1950; Coulson, 1988).

It is remarkable that in spite of the clarity of this theory, several measurements of earlier students of total eclipses contradict with it. One can mention, e.g., Dandekar and Turtle (1971), who conducted skylight polarization measurements at 90° from the sun on the antisolar meridian. Their polarimeter had a field of view of 5°. They observed that the polarization reached a minimum of 4.0% at $\lambda = 475$ nm (blue) and was less than 0.6% at $\lambda = 600$ nm (red) during the total eclipse of 7 March 1970 in Kinston, USA. On the basis of the above-mentioned general rule, it is clear that also during the total eclipse of 7 March 1970, the degree of polarization of skylight should have been lower in the blue spectral range than in the red one.

Thus, the spectral measurements of Dandekar and Turtle (1971) should have been erroneous, the reason for which might have been an incorrect calibration of their polarimeter, for example. Although they stated that "all the instruments were calibrated against a source of known spectral distribution," they did not describe any detail of this calibration. As Dandekar and Turtle wrote: "Well outside the period of totality, the polarization was about 42% with no significant difference between the two colours." This demonstrates well that their polarimeter was incorrectly calibrated and/or not sensitive enough because it should have been able to measure the above-mentioned, rather strong, reduction of the degree of polarization of skylight in the blue spectral range in comparison with the smaller decrease of the degree of polarization in the red range of the spectrum.

According to Dandekar and Turtle (1971): "Polarization observations for a total solar eclipse have been previously conducted by de Bary et al. (1961) and Moore and Rao (1966). Outside the period of totality, all observed the red polarization to be weaker than the blue polarization, which is in agreement with the theory." However, we have shown above that this just contradicts with the theory. In the opinion of Dandekar and Turtle "at totality, with the primary scattering absent in the umbral region, the shorter wavelengths should still suffer stronger polarization." This explanation of their observation is, however, erroneous again because from the theory of multiple scattering, it follows that also at totality, in the umbral region, the shorter wavelengths should suffer weaker polarization.

The spectral dependence of the polarization measured by Dandekar and Turtle (1971) during totality was in contradiction also with the observations of Moore and Rao (1966), who observed a polarization of 0.5% and 4.5% for the blue (400 nm) and the red (600 nm) spectral range, respectively, for the 30 May 1965 eclipse. They attributed their "anomalous dispersion" of polarization to the presence of a diffusely reflective cirrus cloud deck beneath the aircraft. However, on the basis of the above theoretical considerations and also of our results presented in this work on the dispersion of the polarization of skylight during totality, we must conclude that Dandekar and Turtle measured an "anomalous dispersion" (in all probability due to an incorrect spectral calibration of their polarimeter) and not Moore and Rao.

4.3.2.2. Celestial ***E****-vector pattern during totality.* According to Können (1985, pp. 38–40), during total solar eclipses, the direction of "polarization is... no longer

tangential with respect to the sun, because the latter does no longer act as the main source of light... Just as in the case of ordinary twilight, the source of light can be thought to be on the horizon and an additional scattering by air particles results in vertical polarization. But since this multiply scattered light is now completely dominant, its vertical polarization shows up all over the sky... The distribution of the... polarization is symmetrical with respect to the zenith."

It is clear from Figs. 2A–C, 3, 4, 5, and 7 that several details of the above general description of the celestial polarization pattern during total eclipses are erroneous.

(1) Vertical (i.e., approximately parallel to the local meridian) polarization (shaded by dark grey or bright grey in the patterns of the ***E***-vector alignment of skylight in this work) does not show up all over the sky during totality. We can see in Fig. 2C3–C5 that during totality, almost the entire antisolar hemisphere of the sky was characterized by ***E***-vector alignments more or less perpendicular to the local meridian (shaded by middle grey).

(2) During totality, the celestial distribution of the direction of polarization (i.e., the ***E***-vector alignment) of skylight is not symmetrical at all with respect to the zenith, and the pattern of the degree of polarization of skylight is not exactly rotationally symmetric to the zenith, as can be clearly seen in Figs. 2B3–B5,C3–C5, 5B3–B5,C3–C5, and 7.

Theoretically, the distribution of skylight polarization during a total eclipse possesses an exact cylindrical symmetry only in that case if (1) the moon's shadow is cylindrical; (2) it is vertical (i.e., perpendicular to the horizontal Earth's surface); and (3) the observer is at the centre of the circular umbra. It is evident that prerequisites (1) and (2) are satisfied very rarely (if ever), and prerequisite (3) can be fulfilled only for a single moment, if the observer is placed on the centre line of the path of the umbra. At this single moment, the ***E***-vector alignment of skylight is predominantly horizontal (and not vertical) over the entire celestial firmament, because then, at any point in the atmosphere, the ***E***-vector alignment is perpendicular to the predominantly vertical plane of scattering determined by the triangle formed by the observer, the point observed, and the approximately radially propagating light coming from outside the umbral zone.

Können (1985) seemed to forget that during total solar eclipses, the variation of the celestial polarization pattern depends strongly on the moving direction of the elliptical umbra relative to the site of the observer and to the geometrical factors, which vary rapidly during the total phase. Thus, the celestial polarization pattern (especially the ***E***-vector pattern) is neither constant nor exactly symmetrical with respect to the zenith or midtotality. Evidence for this was first presented by Shaw (1975), and this is demonstrated also in Figs. 2, 5, 6, and 7 of the present work.

The above-mentioned discrepancies of certain earlier eclipse measurements and interpretations, and the fact that some previous eclipse observations are in contradiction with the theory, as well as other observations show that until now, there was not enough information available about the celestial polarization pattern during total solar eclipses. However, full-sky (180° field of view) imaging polarimetry can help to gather as much information as needed for a comprehensive theory and computer simulations of the polarization characteristics of multiply scattered skylight during eclipses.

4.4. Need for theoretical analyses and computational studies on the spatiotemporal change of the celestial polarization pattern during total solar eclipses

Shaw (1975) developed a rough radiative transfer model for the eclipse geometry, which treats scattering of second order. His modeling efforts were, however, restricted to scalar fields of brightness and colour of skylight and did not treat skylight polarization.

The change of sky polarization that occurs during totality is complex and depends on the distribution and magnitude of numerous parameters. Among these, we mention variations in ground albedo, solar zenith angle, shape and diameter of the eclipse shadow, optical thickness of the atmosphere, and the distribution and extent of the cloud cover (if any). In view of the complex geometry and the number of mitigating parameters (many of which are unknown), we have attempted to explain and interpret certain polarization characteristics during totality only in a general and qualitative way. It would be desirable to interpret our results in terms of a theory that would clearly define the various atmospheric, geometrical, and terrain factors determining the celestial polarization pattern during a total eclipse. As far as we know, a definitive theory is not yet available; there has been practically no work reported on modeling of the radiative transfer processes that occur in the geometry of a total eclipse.

In the past, several authors have carried out detailed computations including the secondary and higher orders of scattering for a purely molecular atmosphere for determining sky brightness, colour, and polarization for a normal day (reviewed, e.g., by Coulson, 1988). The quantitative estimates become complicated due to the anisotropy of the scattering particles, ground reflection, processes of absorption and extinction, and also the non-Rayleigh scattering events due to large suspended particles such as haze, dust, and aerosols. As a result, uncertainties and variations in these quantities have resulted in rather unsatisfactory agreement between theory and observations. The situation is further complicated by the complex geometry of the shadow region for the period of totality of the solar eclipse. Thus, to our knowledge, there exists no computation for determining the sky polarization during an eclipse. We, therefore, have presented the results of our imaging polarimetric measurements as experimental in nature and have not attempted a

quantitative theoretical evaluation. Nevertheless, we gave a sound qualitative analysis of the origin of the ***E***-vector pattern and the zenith neutral point, as well as the spectral dependence of skylight polarization during totality.

Until now, insufficient wide-field observational data on sky polarization during eclipses have been accumulated. However, using 180° field-of-view imaging polarimetry, enough observational data can be gathered during future total eclipses, covering a wide range of each of the relevant eclipse parameters, such as the solar zenith angle, altitude, celestial distribution of brightness, colour, and polarization of multiply scattered skylight. These data build the basis of a theory that should be developed urgently in order to interpret quantitatively all eclipse observations. We hope that our results, presented in this work, may encourage the establishment and development of such a theory.

Acknowledgements

This work was supported by a 3-year János Bolyai postdoctoral research fellowship received by G. Horváth from the Hungarian Academy of Sciences, and by a 1-year doctoral research fellowship received by J. Gál from the George Soros Foundation (grant no. 230/2/878). The grants OTKA F-025826 and T-034981 received by G. Horváth from the Hungarian National Science Foundation, and 31-43317.95 received by R. Wehner from the Swiss National Science Foundation are gratefully acknowledged. Many thanks are due to Mária Fischer and János Horváth for their assistance during the measurements in Kecel. Thanks are due to three anonymous referees for their comments and suggestions.

References

Chandrasekhar, S. (1950). *Radiative transfer*. Oxford: Clarendon Press.

Coulson, K. L. (1988). *Polarization and intensity of light in the atmosphere*. Hampton, VA: A. Deepak Publishing.

Dandekar, B. S., & Turtle, J. P. (1971). Day sky brightness and polarization during the total eclipse of 7 March 1970. *Applied Optics*, *10*, 1220–1224.

de Bary, E., Bullrich, K., & Lorenz, D. (1961). Messungen der Himmelsstrahlung und deren Polarisationsgrad während der Sonnenfinsternis am 15.2.1961 in Viareggio. *Geofisica Pura et Applicata*, *48*, 193–198.

Gál, J., Horváth, G., & Meyer-Rochow, V. B. (2001). Measurement of the reflection–polarization pattern of the flat water surface under a clear sky at sunset. *Remote Sensing of Environment* (in press).

Horváth, G., Gál, J., Pomozi, I., & Wehner, R. (1998). Polarization portrait of the Arago point: video-polarimetric imaging of the neutral points of skylight polarization. *Naturwissenschaften*, *85*, 333–339.

Horváth, G., & Varjú, D. (1997). Polarization pattern of freshwater habitats recorded by video polarimetry in red, green and blue spectral ranges and its relevance for water detection by aquatic insects. *Journal of Experimental Biology*, *200*, 1155–1163.

Horváth, G., & Wehner, R. (1999). Skylight polarization as perceived by desert ants and measured by video polarimetry. *Journal of Comparative Physiology, A*, *184*, 1–7 (Erratum 184, 347–349 (1999)).

Können, G. P. (1985). *Polarized light in nature*. Cambridge: Cambridge Univ. Press.

Moore, J. G., & Rao, C. R. N. (1966). *Annales Geophysicae*, *22*, 147.

North, J. A., & Duggin, M. J. (1997). Stokes vector imaging of the polarized skydome. *Applied Optics*, *36*, 723–730.

Rao, C. R. N., Takashima, T., & Moore, J. G. (1972). *Journal of Atmospheric and Terrestrial Physics*, *34*, 573.

Sharp, W. E., Silverman, S. M., & Lloyd, J. W. F. (1971). Summary of sky brightness measurements during eclipses of the sun. *Applied Optics*, *10*, 1207–1210.

Shaw, G. E. (1975). Sky brightness and polarization during the 1973 African eclipse. *Applied Optics*, *14*, 388–394.

Voss, K. J., & Liu, Y. (1997). Polarized radiance distribution measurements of skylight: I. System description and characterization. *Applied Optics*, *36*, 6083–6094.